

## Structural, Chemical, and Electronic State on $\text{La}_{0.7}\text{Sr}_{0.3}\text{MnO}_3$ Dense Thin-film Surfaces at High Temperature – *Surface Segregation*

Helia Jalili, Yan Chen, and Bilge Yildiz

Laboratory for Electrochemical Interfaces

Massachusetts Institute of Technology, 77 Massachusetts Avenue, Cambridge,  
Massachusetts 02139, USA

The evolution of the surface topographic and electronic structure and chemical state of the  $\text{La}_{0.7}\text{Sr}_{0.3}\text{MnO}_3$  (LSMO) thin films were probed using Scanning Tunneling microscopy (STM) and X-ray photoelectron spectroscopy (XPS) at elevated temperature and oxygen gas environment to identify the structural nature of surface segregation of Sr on LSMO. The as-prepared films had a layer-by-layer structure with a step height of 3.9 Å, close to the lattice parameter of LSMO. Up to 500°C, the topography and the step heights remained the same, statistically within 2-4%, implying that no phase separation took place on the top layers of the film. The low oxygen pressures, down to  $10^{-10}$  mbar, at elevated temperatures promoted segregation of Sr by 12-20% on the A-site, accompanied by a smaller increase of (La+Sr)/Mn. Our results suggests two possible structures for Sr segregation; the replacement of La by Sr on the AO-surface of the LSMO which retains a perovskite termination, or a separate AO-oxide phase nucleating on the defected lower layers.

### Introduction

Amongst the various types of fuel cells, the Solid Oxide Fuel Cell (SOFC) is particularly attractive given its fuel flexibility (hydrocarbons, hydrogen or even CO) and high conversion efficiencies enabled by its relatively high operating temperature (800-1000°C). In addition, the SOFCs can work in a reversible mode, for example, coupled to a nuclear plant or concentrated solar power, to produce electricity, and hydrogen or syn-gas for liquid fuels synthesis, alternating the product streams between days and nights. Fundamental understanding of the surface electronic and chemical state of the cathode is needed to enable rational design of materials for intermediate temperature and more durable SOFCs. For this purpose, probing the cathode surfaces at high temperature and  $\text{O}_2$  environment is an asset to relate the surface structure and chemistry to the oxygen reduction kinetics at the atomistic level (1, 2).

The relation of equilibrium surface segregation, that is the enhancement or depletion of a certain cation in the cathode structure at a given temperature and pressure, to oxygen reduction kinetics is an outstanding question. In the perovskite structured cathode material  $\text{La}_{(1-x)}\text{Sr}_x\text{MnO}_3$  the ratio of A site to B site cations (A/B) can deviate from stoichiometric ratios significantly (3), driven for example by an enrichment of Sr or La cations on the surface. However, the origin of the A-site segregation, the structure of the segregated surface, and the temperature and pressure conditions that promote this segregation remain open.

The change of A/B could originate from different mechanisms including Sr enrichment at the A-site, i.e. Sr replacing La on the perovskite terminated surface (4), formation of a separate oxide layer (Sr,La)-O (5), and formation of Ruddlesden Popper

phases ((La,Sr)<sub>2</sub>MnO<sub>4</sub>) (6). Fister et al. (4) reported Sr surface segregation using *in-situ* synchrotron measurements of total reflection fluorescence over a wide range of temperature, T, and oxygen pressure, P<sub>O<sub>2</sub></sub> for La<sub>0.7</sub>Sr<sub>0.3</sub>MnO<sub>3</sub>. He observed the surface segregated Sr increases as oxygen pressure decreases, and interpreted that Sr replaces La on the AO-terminated surface of the perovskite. Fister proposed the surface oxygen vacancy concentration controls the degree of segregation. Another hypothesis about the origin of A-site segregation is the formation of the A-site containing oxides (SrO or La<sub>2</sub>O<sub>3</sub>) separated on the surface, shown by Liu et al (5). High resolution TEM images from the LSMO and other perovskite surfaces clearly showed the formation of an A-oxide on the surface. The last hypothesis that we note here proposes that the A-site rich structure originates from the formation of the layered Ruddlesden Popper phases ((La,Sr)<sub>2</sub>MnO<sub>4</sub>), which was shown using angle resolved x-ray photoelectron spectroscopy on thin LSM films (6).

The objective of our research reported here is to identify the structure of A-site surface segregation on Sr-doped LaMnO<sub>3</sub> with a nominal composition of La<sub>0.7</sub>Sr<sub>0.3</sub>MnO<sub>3</sub> (LSMO) at high temperature and high oxygen pressure. We investigated the changes in A/B site in a controlled way, by *in-situ* treatment and at the atomic level to confirm or exclude the abovementioned mechanisms governing the surface segregation upto 500°C and 10<sup>-3</sup> mbar of oxygen partial pressure.

### Experimental Approach

Scanning tunneling microscopy (STM) was used to investigate the surface morphology and electronic structure at elevated temperatures and oxygen environment. This information was combined with the chemical composition on LSMO using x-ray photoelectron spectroscopy (XPS).

The experiments were performed in a modified ultrahigh vacuum (UHV) system design by Omicron Nanotechnology, Inc., with the base pressure lower than 5×10<sup>-10</sup> Torr. Microscope chamber is equipped with a variable temperature scanning tunneling microscope and non-contact atomic force microscope. The analysis chamber was equipped with a five-channel hemispherical electron analyzer and x-ray source for the XPS. A heater was installed on the manipulator arm that allows us to heat the sample while performing XPS analysis.

The samples in this investigation were epitaxially grown La<sub>0.7</sub>Sr<sub>0.3</sub>MnO<sub>3</sub> on SrTiO<sub>3</sub> substrate using the pulsed laser deposition technique. The as-grown films were cleaned in ultrasonic bath with 99.99% purity ethyl-alcohol, followed by Ar blow drying. In order to remove the carbon contamination, sample cleaning for the STM experiments was performed by heating the samples in oxygen for 30 min at 5×10<sup>-6</sup> mbar in the UHV chamber. This resulted in a significant reduction of the carbon content.

During the cleaning of the samples in oxygen, the high-temperature STM/STS, and the XPS experiments, the sample was radiatively heated by using a Pyrolytic Boron Nitride (PBN) heater. 10<sup>-3</sup> mbar oxygen pressure localized in the vicinity of the sample's surface was created during the STM measurements via direct oxygen dosing by a retractable dozer equipped with high precision leak valve. STM at room temperature (RT) and high temperatures (HT) up to 580 °C was performed in the constant-current mode using Pt/Ir tips. The bias voltage of 1-2 V applied to the sample during STM measurement and the tunneling current, *I*, ranged from 50-500 pA.

## Results and Discussion

### Surface Phase on LSMO Film

Effect of the annealing in the non-UHV partial pressure of oxygen and in UHV at temperatures up to 580 °C was studied in consecutive steps of temperature. Figure 1(a,b) shows the room temperature STM image of the as-grown film of LSM/STO after a 30 min heating in oxygen pressure of  $10^{-6}$  mbar at 500 °C to clean its surface. Figure 1(a) shows the morphology of the surface over large area of  $500 \times 500 \text{ nm}^2$ . Surface is smooth with well resolved step edges. Figure 1(b) shows the zoomed-in image and the white line corresponds to the position of the height profile taken. Figure 1(c) shows that the step height between each layer is  $3.9 \pm 0.2 \text{ \AA}$ . The potential phases that can form on the surface of the LSM film with their respective lattice constants are summarized in Table (1). Comparing the lattice parameters of the compounds listed in Table 1 and the step height between each layer obtained from the STM measurements, we found that the LSMO lattice parameter has the closest match ( $3.88 \text{ \AA}$ ) to the measured step height differences. This implies that the LSMO surface consists of several monolayers of LSMO before being subject to oxidizing or reducing under controlled conditions. However, the bottom most layer exposed on the surface is not as smooth as the top layers and it has a defected structure. The smooth and well-defined top layers will be used in the next sections as a reference from which the surface may deviate upon cation segregation on the surface.

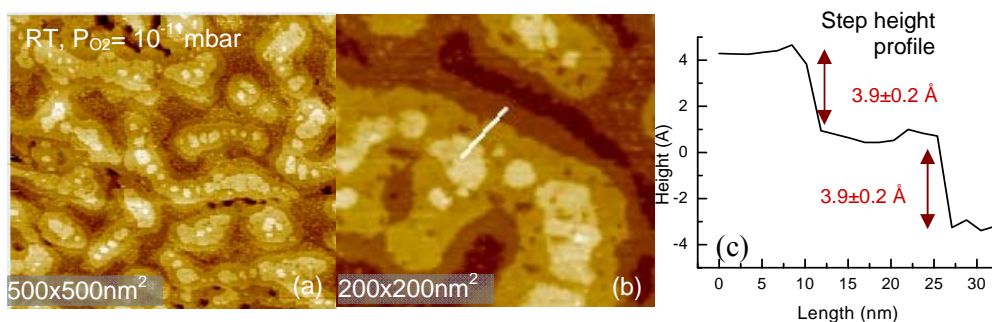


**Figure 1:** LSM surface morphology, and step height analysis of the 10 nm thick LSMO thin film grown on STO substrate. (a) Large area  $500 \times 500 \text{ nm}^2$  image, (b) the zoomed-in image for clarity on the step height analysis, (c) the cross sectional height-profile measured from (b), with a height difference between each step as  $3.9 \pm 0.2 \text{ \AA}$ .

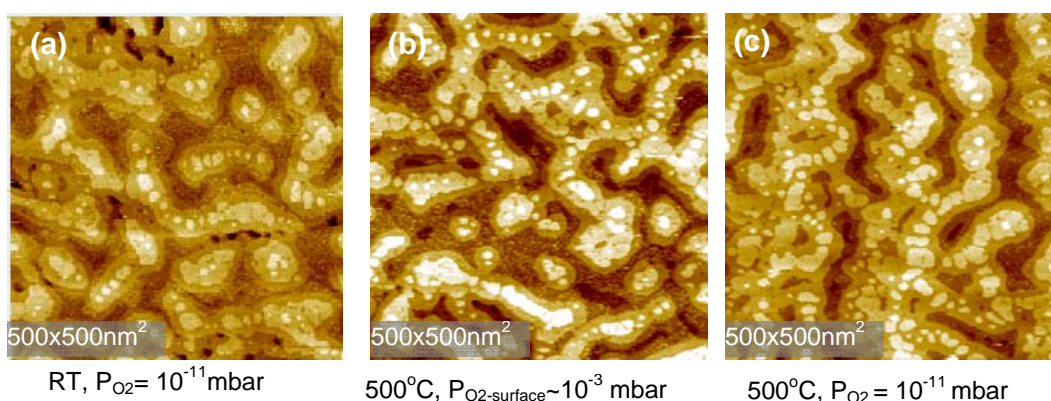
**Table 1:** Possible phases that can stabilize on the LSMO surface and their respective lattice parameters.

Compound	Lattice parameters
<sup>(7)</sup> $\text{La}_{0.7}\text{Sr}_{0.3}\text{MnO}_3$	$a=b=c=3.88 \text{ \AA}$
<sup>(8)</sup> $\text{SrO}$	$a=b=c=5.16 \text{ \AA}$
<sup>(9)</sup> $\text{SrCO}_3$	$a=5.1, b=8.4, c=6.0 \text{ \AA}$
<sup>(10)</sup> $\text{La}_2\text{O}_3$	$A=b=3.4, c=6.1 \text{ \AA}$
<sup>(11)</sup> $(\text{La,Sr})_2\text{MnO}_4$	$a=b=3.84, c=12.5 \text{ \AA}$

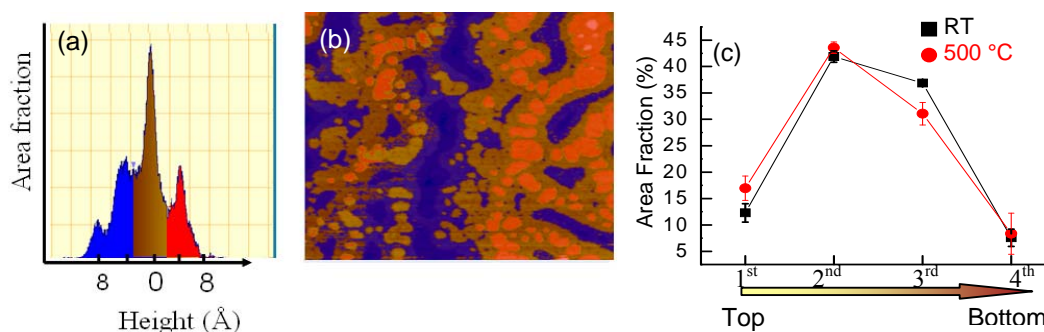
### Measure of Phase Separation with Temperature and $P_{\text{O}_2}$

Figure 2 shows the surface morphology of the LSMO at three different conditions, (a) RT and UHV pressure, (b)  $T = 500^\circ\text{C}$  and  $P_{\text{O}_2\text{-surface}} \sim 10^{-3}$  mbar, and (c)  $500^\circ\text{C}$ ,  $P_{\text{O}_2} = 10^{-11}$  mbar. No distinct change in surface morphology was observed upon

annealing upto 500 °C. Even at high temperature of 580 °C, the step size between each layer remained the same ( $3.9 \pm 0.2$  Å) when in oxygen pressure. Results shown in Figure 2 indicated no evidence of secondary phase formation that was detectable in morphology and/or change of the step size between each layer. In order to quantitatively and more accurately analyze the size distribution from Figure 2, we took a statistical approach. For this purpose, we applied the Histogram analysis using the SPIP image and data analysis software (12). Figure 3 (a) shows the histogram obtained for Figure 2(c). Each peak in the histogram (Figure 3(a)) corresponds to the height of each layer, and the integral of each peak determines the area fraction contributed by each layer. For the specific case that was shown in Figure 3(a), from right to left, the first peak located at 8 Å, arise from the contribution of the top-most layer, the second peak corresponds to the second top layer and so on. To get good statistics, the analysis was performed for about 20 different images each at RT (black curve) and at HT (red curve). These results are summarized in Figure 3(c). As shown in Figure 3(c), there is only a small difference (2-4%) between the size distribution at HT and RT.



**Figure 2:** Surface morphology of the 10 nm LSM on STO (a) at room temperature after cleaning the surface, (b) at 500° C in oxygen ( $P_{O_2}=10^{-3}$  mbar), (c) at 500 °C in oxygen ( $P_{O_2}=10^{-11}$  mbar).



**Figure 3:** (a) and (b) show the STM image and the corresponding histogram diagram representing the area fraction of each layer, (c) summarizes the quantified size distribution of each layer at RT (Black curve) and HT (Red curve). For each temperature, these data were obtained from histograms as shown in (a).

### Chemical Composition on LSMO Film

To capture the changes in chemical state arising during and posterior to the annealing process, and correlate these to the structural changes summarized in Figure 3, we performed XPS measurements on the as-received and the annealed samples. Figure 4(a) on the left side (black curve) shows the ratio of the content of A-site cations to B site cations,  $(La+Sr)/Mn$ , and on the right side (red curve) shows the ratio of Sr to A site  $(Sr/(Sr+La))$  for four different treatments; at RT and HT for the UHV annealed sample as well as the oxygen annealed sample. Figure 4(a) indicates several interesting points: 1- The starting condition of the surface is A-site rich. Given the step-height corresponding to the LSMO lattice parameter, we deduce that the surface is made of AO-terminated perovskite layers. 2- Annealing the sample in UHV and/or oxygen promotes an increase of A-site. 3- Increase of Sr is more evident on the UHV-annealed sample compared to the oxygen-annealed sample. Figure 4(b) shows the oxygen content relative to the cations. As one would expect, the surface oxygen content decreases as the pressure reduces, nevertheless, surface oxygen was present even at HT and UHV conditions, implying that the surface was not reduced to a state including only the metal cations.

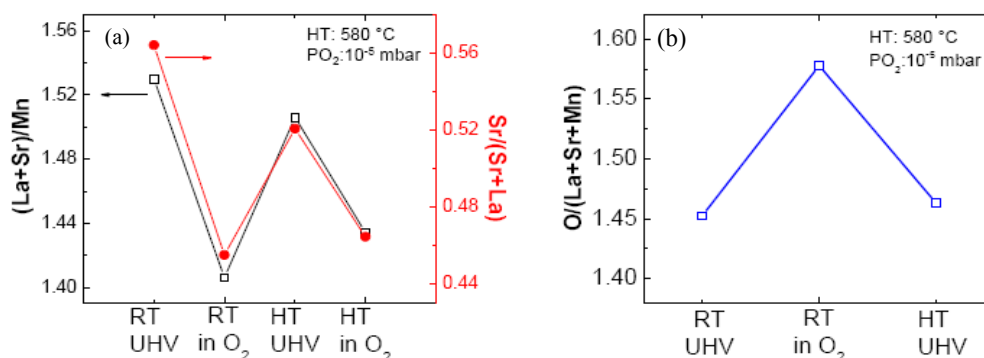


**Figure 4:** The XPS data obtained for LSMO/STO at different conditions of RT and HT in UHV and oxygen partial pressure. (a) Black curve: ratio of A to B site, Red curve: ratio of Sr to A site. (b) Ratio of oxygen to the rest of the cations.

In order to deduce the nature of the segregation and the surface structure upon segregation, data from histogram analysis was compared with the XPS data. XPS data revealed 12-20% relative change in the Sr content on the A-site during the treatments of the surface at various temperatures and oxygen pressures. The STM statistical analysis showed only a small difference (2-4%) between the size distribution at HT and RT, and no other changes in the morphology on the flat top layers were observed. Comparing the 12-20% chemical change with the max 2-4% change in the area of the surface layers suggests that the A-site and Sr-site rich surface can not arise due to a secondary phase formation as a separate oxide phase on the top layers of the LSMO film in the conditions we tested. Also considering the fact that the step sizes between each layer stayed the same (3.9 Å) regardless of T and PO<sub>2</sub>, we also rule out the possibility of Ruddlesden Popper phase,  $(La,Sr)_2MnO_4$  with a z-axis lattice constant of  $c=12.5$  Å. The only mechanism that we can not rule out based on our current results is the replacement of La by Sr on the A-O terminated surface that retains its perovskite layered structure upto 500 °C. However, due to defected nature of the bottom layer of the surface morphology that makes limits resolution limit of the present measurements, we have not excluded the possibility of Sr surface segregation as a separate phase on the bottom defected layer.

### Concluding Remarks

Evolution of surface morphology, electronic structure and chemical state was studied as a function of temperature and oxygen pressure using STM and XPS. The STM showed that the surface had a layer-by-layer structure with a step height of 3.9 Å, close to lattice parameter of LSMO. Two different morphologies were depicted. Top layers were flat with roughness less than 0.1 nm whereas the bottom layer was defected, making it difficult to resolve possible secondary phase formation on the bottom layer. At high temperature of 500 °C and oxygen pressures of  $10^{-10}$ - $10^{-3}$  mbar, no evident change of morphology was observed, and the layered nature of the surface and step height remained the same.

The XPS data and analysis indicated that the low  $P_{O_2}$  (UHV) environment promotes segregation of A-site with a pronounced change on the Sr content. The significant changes on the Sr content, accompanied by only a small change on the surface morphology suggests two possible structures for Sr segregation on LSMO in the T and  $P_{O_2}$  conditions reported here; the replacement of La by Sr on the AO-surface of the LSMO which retains a perovskite termination; or a separate AO-oxide phase nucleating on the defected lower layers. High resolution STM with refined XPS analysis will be performed to resolve these two possible structures at the atomistic scale.

### Acknowledgments

Authors thank Paul Salvador's group at Carnegie Mellon University for providing the samples in this study, Prof. Heske's group at University of Nevada Las Vegas for their constructive comments and stimulating discussions. Department of Energy, Office of Fossil Energy for supporting this project under award number DE-NT0004117.

### References

1. Adler S.B., *Chem Rev*, **104**, 4791 (2004).
2. Baumann F.S., Fleig J., Konuma M., Starke U., Habermeier H.U. and Maier J., *J. Electrochem. Soc.*, **152**, A2074 (2005).
3. Katsiev K., Yildiz B., Balasubramaniam K. and Salvador P.A., *Appl. Phys. Lett.*, **95**, - (2009).
4. Fister T.T., Fong D.D., Eastman J.A., Baldo P.M., Highland M.J., Fuoss P.H., Balasubramaniam K.R., Meador J.C. and Salvador P.A., *Appl. Phys. Lett.*, **93**, 151904 (2008).
5. Private communication with Prof. Meilin Liu, Georgia Tech University.
6. Dulli H., Dowben P.A., Liou S.H. and Plummer E.W., *Phys Rev B*, **62**, 14629 (2000).
7. Martin M.C., Shirane G., Endoh Y., Hirota K., Moritomo Y. and Tokura Y., *Phys Rev B*, **53**, 14285 (1996).
8. Bertacco R., Contour J.P., Barthelemy A. and Olivier J., *Surf Sci*, **511**, 366 (2002).
9. Thongtem T., Tipcompor N., Phuruangrat A. and Thongtem S., *Mater. Lett.*, **64**, 510-512 (2010).
10. Hu C.G., Liu H., Dong W.T., Zhang Y.Y., Bao G., Lao C.S. and Wang Z.L., *Adv. Mater.*, **19**, 470 (2007).
11. Zheng F. and Pederson L.R., *J. Electrochem. Soc.*, **146**, 2810 (1999).
12. <http://www.nanoscience.com>.